

# Adaptive Reduced-Order-Model-Based Control-Law Design for Active Flutter Suppression

Gang Chen,<sup>\*</sup> Jian Sun,<sup>†</sup> and Yue-ming Li<sup>‡</sup>

*Xi'an Jiaotong University, 710049 Xi'an, People's Republic of China*

DOI: 10.2514/1.C031236

The design of classic active flutter controllers has often been based on low-fidelity and low-accuracy linear aerodynamic models. Most of these models were usually treated as a linear time-invariant system, without considering time-varying parameters, such as the Mach number, the angle of attack, the Reynolds numbers, etc. A high-fidelity reduced-order model based on the proper orthogonal decomposition adaptation algorithm is used to develop a new general linear parameter-varying aeroservoelastic model with aerodynamic nonlinearity. A robust gain-scheduling control-law design method for active flutter suppression based on the proposed linear parameter-varying model is investigated. The proposed design method is demonstrated with the Goland+ wing aeroelastic model. The simulation results show that the linear parameter-varying gain-scheduled controller can effectively suppress flutter over a range of airspeeds, and the flutter boundary in the transonic regime is simultaneously increased by nearly 20% to 30%.

## Nomenclature

$A$	=	volume of the fluid cell
$\mathbf{F}$	=	flux value
$f, g$	=	generic functions
$K$	=	control gain
$q$	=	dynamic pressure
$R$	=	proper orthogonal decomposition kernel matrix
$u$	=	structural displacement
$v$	=	structural velocity
$W$	=	snapshot matrix
$\Delta w, \Delta u, \Delta \dot{u}$	=	perturbations of the steady-flow values
$\beta$	=	deflection of the control surface
$\Psi_r$	=	proper orthogonal decomposition basis

## I. Introduction

FLUTTER is a dynamic instability caused by the interaction of structural, inertial and aerodynamic loads that can lead to the sudden mechanical failure of an aircraft wing during flight. Because of the severity of the potential emergence failure, a real aircraft typically operates in the region well below the flutter boundary. The tendency to reduce the weight and increase the structural flexibility and operating speed of aircraft with lightweight composite materials greatly increases the possibility of flutter occurrence within the aircraft operational envelope. The active control of nonlinear aeroelastic instability, such as active flutter suppression, is becoming a promising and attractive technology because it can simultaneously reduce the weight and increase the performance of modern aircraft [1].

Presented at the 52nd AIAA/ASME/ASCE/AHS/ASC Structures, Structural Dynamics and Materials Conference, Denver, CO, 4–7 April 2011; received 12 September 2010; revision received 7 December 2011; accepted for publication 13 December 2011. Copyright © 2011 by the American Institute of Aeronautics and Astronautics, Inc. All rights reserved. Copies of this paper may be made for personal or internal use, on condition that the copier pay the \$10.00 per-copy fee to the Copyright Clearance Center, Inc., 222 Rosewood Drive, Danvers, MA 01923; include the code 0021-8669/12 and \$10.00 in correspondence with the CCC.

<sup>\*</sup>Associate Professor, Department of Aerospace Engineering, School of Aerospace, State Key Laboratory for Strength and Vibration of Mechanical Structures.

<sup>†</sup>Assistant Professor, Department of Aerospace Engineering, School of Aerospace, State Key Laboratory for Strength and Vibration of Mechanical Structures (Corresponding Author).

<sup>‡</sup>Chair of the Department of Scientific and Engineering Computing, School of Aerospace, State Key Laboratory for Strength and Vibration of Mechanical Structures.

The design of classic active flutter controllers is usually based on low-fidelity linear aerodynamic models, such as Theodorsen's quasi-steady aerodynamic model [2,3], the lift-surface theory, and the doublet-lattice method used in the ZEARO software system [4]. These low-fidelity models have led to great achievements in the design of classic flutter controllers, especially in the low-speed subsonic regime. However, these methods (i.e., panel methods) require good prior knowledge and experience regarding the characteristics of the aeroelastic system. The generalized unsteady aerodynamic forces must be calculated for each structural mode over a wide range of frequencies; then, they must be transformed into the time domain to construct the aeroservoelastic model by the rational-function approximation [5], which is a tedious process. The greatest shortcoming of this approach is that the low-fidelity linear aerodynamic model cannot accurately capture the dominant nonlinear unsteady behaviors of the flow in the transonic regime, such as shock movement and flow separation, which have significant impacts on the aeroelastic responses.

As a benefit of the development of computational aeroelasticity, the nonlinear aeroelastic response can be accurately predicted by the high-fidelity physics-based fluid-structure coupling solver, such as the computational fluid dynamics (CFD) solver and computation structural dynamics (CSD) solver. However, the use of multistep time-domain calculations for each aircraft state is computationally expensive. The high dimensionality of the full-order CFD model also prevents its application to controller design. To reduce the expensive computational cost and the high order of the CFD model, a novel concept called the reduced-order model (ROM) has been proposed in recent years. The ROM seeks to capture the dominant nonlinear behaviors of the aeroelastic system with the use of a simple mathematical representative model constructed from the full-order system. The use of this model is convenient in conceptual design, control, and data-driven systems [6]. Different approaches for the reduced-order modeling of aerodynamic systems have been proposed, including system-identification-based data-driven models, such as the Volterra theory of nonlinear systems [7] and the linear model-fitting ARMA model [8], as well as flow eigenmode-based models, such as the proper orthogonal decomposition (POD) method [9,10] and the nonlinear dynamic-theory-based models [11,12]. Both the Volterra/ROM and POD/ROM methods recently have been used to design active control laws for suppressing two-freedom aeroelastic systems [13], BACT models [14,15], and wing models [16,17].

Many types of classic and modern control theories have been applied to the design of active control laws [1,13–17]. The designs of most of these control laws are based on linear time-invariant (LTI) models. The LTI-based controllers must be designed at several

previously selected operating points and combined with another explicit gain-schedule controller during their operation. Because of the lack of a systematic stability analysis method, the control performance of such controllers in the entire flight envelope cannot be ensured a priori. Actually, the flow parameters (for example, the dynamic pressure, Mach number, angle of attack, etc.) are usually time-varying in operation, and these parameters have a great impact on the aeroelastic response. Gain-scheduled linear parameter-varying (LPV) control is a natural extension of  $H_\infty$  control for systems that vary smoothly as a function of the chosen scheduling parameters. LPV models can offer many advantages that are not available from the single operating-point-based LTI models. If the parameters of the LPV model can be measured in real time, the LPV control theory can then be used to design an automatically gain-scheduled stable controller that depends on the same parameters, and no ad hoc gain-scheduling methods are required [18]. LPV control of aeroelastic systems has been investigated by several researchers. Barker et al. successfully designed a robust control law based on the LPV model by linear fractional control [19]. However, Barker's LPV model is constructed from a simple direct linear interpolation of many LTI models built in different Mach numbers and dynamic pressures. It is not suitable for nonlinear aeroelastic systems in the transonic regime. Prime et al. have shown that the LPV controller can autoschedule with the airspeed and effectively suppress the limit-cycle oscillations of the three-degrees-of-freedom airfoil aeroelastic system over a range of airspeeds [3]. Their LPV model is based on Theodorsen's low-fidelity quasi-steady aerodynamic model, which is also not easily applicable to three-dimensional nonlinear aeroelastic systems, especially in the transonic regime.

Recently, we have investigated physics-based high-fidelity low-order aeroservoelastic models, which were used to design an active control law for the Golland+ wing based on the Volterra-ROM [16] and for the AGARD 445.6 wing based on the POD-BT-ROM [17] combined with the linear-quadratic regulator (LQR) method. The traditional ROM is sensitive to variation of the flow parameter; thus, the stability and performance of the LQR controller cannot be ensured when the flow parameters vary during flight operation. To maintain the prediction accuracy of the aeroservoelastic model, we can construct several POD-ROMs over a wide range of the flight envelope at specified intervals and quickly reconstruct a new ROM by interpolating the precalculated POD-ROMs. In this paper, we investigate a new general LPV aeroelastic model based on the POD adaptation method first proposed by Lieu et al. [20]. As a demonstration, an LPV controller will be designed for the Golland+ wing based on the LPV aeroelastic model and used to actively suppress the dynamic instability with flow-parameter variation.

## II. Adaptive POD-ROM Model for Aeroelastic System

### A. Dynamic Linearized Equation for the Aeroelastic System

For a fully coupled nonlinear aeroelastic system, the Euler/Navier–Stokes equation discretized by the finite volume method is written as follows:

$$(A(u)w)_t + F(w, u, \dot{u}) = 0 \quad (1)$$

where  $w$  is the conservative flow variable,  $F$  is the flux,  $A$  is the volume of the fluid cell, and  $u$  is the displacement of the structural grids. Supposing that  $\Delta w$ ,  $\Delta u$ , and  $\Delta \dot{u}$  are small perturbations around the steady state variables  $(w_0, u_0, \dot{u}_0)$ , we can obtain the following linearized equation [20]:

$$A_0 \delta \dot{w} + H \delta w + G \delta u + (C + E) \delta \dot{u} = 0 \quad (2)$$

$$\begin{aligned} H &= \frac{\partial F}{\partial w}(w_0, u_0, \dot{u}_0) & G &= \frac{\partial F}{\partial u}(w_0, u_0, \dot{u}_0) \\ C &= \frac{\partial F}{\partial \dot{u}}(w_0, u_0, \dot{u}_0) & E &= w_0 \frac{\partial A}{\partial u}(u_0) \end{aligned} \quad (3)$$

where  $A_0$  is the volume of the fluid cell in the steady state. To simplify the notation of the linearized equation,  $w$ ,  $u$ , and  $\dot{u}$  are used to represent the perturbation variables  $\Delta w$ ,  $\Delta u$ , and  $\Delta \dot{u}$ , respectively.

The structural dynamic equation without damping can be written as follows [21]:

$$\begin{cases} Mv_{,t} + f^{\text{int}}(u, v) = f^{\text{ext}}(u, w) \\ f^{\text{int}}(u, v) = K_0 \\ f^{\text{ext}}(u, w) = \frac{\partial f^{\text{ext}}}{\partial u}(u_0, w_0)u + \frac{\partial f^{\text{ext}}}{\partial w}(u_0, w_0)w \end{cases} \quad (4)$$

where  $M$ ,  $f^{\text{int}}$ , and  $f^{\text{ext}}$  are the mass matrix, the structural inner force, and the nonlinear external fluid forces acting at the structural grid points, respectively. If  $v = \dot{u}$ ,  $P = (\partial f^{\text{ext}}/\partial w)(u_0, w_0)$ , and  $K_s = K_0 - (\partial f^{\text{ext}}/\partial u)(u_0, w_0)$ , then the linearized flow equation or the snapshot Eq. (2) can be transformed into the following state-space equation:

$$\begin{cases} \dot{w} = Aw + B[v \quad u]^T \\ F = Cw \end{cases} \quad (5)$$

where  $A = -A_0^{-1}H$ ,  $B = -A_0^{-1}(E + C \quad G)$ , and  $C = P$ . The fully coupled linearized aeroelastic system equation is obtained by combining the structure and fluid equations as follows:

$$\begin{bmatrix} \dot{w} \\ \dot{v} \\ \dot{u} \end{bmatrix} = \begin{bmatrix} -A_0^{-1}H & -A_0^{-1}(E + C) & -A_0^{-1}G \\ M^{-1}P & -M^{-1}C & -M^{-1}K_s \\ 0 & I & 0 \end{bmatrix} \begin{bmatrix} w \\ v \\ u \end{bmatrix} \quad (6)$$

The CFD-based computation of Eq. (6) is too expensive for the near-real-time simulation of flexible aircraft, and it is impractical for controller design because of the large order of the equation. Therefore, the POD approach is used to reduce the full-order aeroelastic system.

### B. POD-ROM of the Aeroelastic System

For one series of data  $\{x^k\}$ ,  $x^k \in 1/2^n$  in the  $n$ -dimensional space, the POD method searches an  $m$ -dimensional proper orthogonal subspace  $\Psi \in R^{n \times m}$  to minimize the mapping errors from  $\{x^k\}$  to  $\Psi$  [22], where

$$G = \min_{\Phi} \sum_{k=1}^m \|x^k - \Phi \Phi^H x^k\| = \sum_{k=1}^m \|x^k - \Psi \Psi^H x^k\|, \quad \Phi^H \Phi = I \quad (7)$$

Equation (7) is equivalent to

$$H = \max_{\Phi} \sum_{k=1}^m \frac{\langle (x^k, \Phi)^2 \rangle}{\|\Phi\|^2} = \sum_{k=1}^m \frac{\langle (x^k, \Psi)^2 \rangle}{\|\Psi\|^2}, \quad \Phi^H \Phi = I \quad (8)$$

The constraint optimization problem of Eq. (8) is transformed into the following Lagrange equation:

$$J(\Phi) = \sum_{k=1}^m \langle (x^k, \Phi)^2 \rangle - \lambda(\|\Phi\| - 1) \quad (9)$$

Solving the partial-derivative objective function  $J(\Phi)$  with respect to  $\Phi$  produces

$$\frac{d}{d\Phi} J(\Phi) = 2XX^H \Phi - 2\lambda \Phi \quad (10)$$

where  $X = \{x^1, \dots, x^m\}$  is the matrix of snapshots. Equation (10) is set equal to zero; thus,

$$(XX^H - \lambda I)\Psi = 0 \quad (11)$$

Equation (11) is a real symmetry eigenvalue problem of the POD kernel  $K = XX^H$ . For high-order  $K \in R^{n \times n}$ , the large eigenvalue problem is not easy to solve. Because  $XX^H$  and  $X^H X$  have the same eigenvalues,  $\Psi$  can also be calculated from the following lower  $m$ -dimensional problem:

$$\begin{cases} X^H X V = V \Lambda \\ \Psi = X V \Lambda^{-1/2} \end{cases} \quad (12)$$

where  $\Psi = (\psi_1, \psi_2, \dots, \psi_m)$ ,  $\Lambda = (\lambda_1, \lambda_2, \dots, \lambda_m)$ , and  $\lambda_1 \geq \lambda_2 \geq \dots \geq \lambda_m$ . By truncating  $\Psi$  to the  $r$ -order vector  $\Psi = (\psi_1, \psi_2, \dots, \psi_r)$ , we can obtain the following reduced-fluid model:

$$\begin{cases} \dot{w}_r = \Psi_r^T A \Psi_r w_r + \Psi_r^T B y \\ F = P \Psi_r w_r \end{cases} \quad (13)$$

Finally, the traditional  $r$ -order time-domain POD/ROM of the aeroelastic system can be represented as follows:

$$\begin{bmatrix} \dot{w}_r \\ \dot{v} \\ \dot{u} \end{bmatrix} = \begin{bmatrix} -\Psi_r^T A_0^{-1} H \Psi_r & -\Psi_r^T A_0^{-1} (E + C) & -\Psi_r^T A_0^{-1} G \\ \frac{1}{2} \rho_\infty V_\infty^2 \bar{M}^{-1} P \Psi_r & -\bar{M}^{-1} \bar{C} & -\bar{M}^{-1} \bar{K}_S \\ 0 & I & 0 \end{bmatrix} \begin{bmatrix} w_r \\ v \\ u \end{bmatrix} \quad (14)$$

The order of the reduced system in Eq. (14) is much smaller than that of the original system in Eq. (6). It can be reduced further, from hundreds to tens, by the balance-truncation method [17]. The POD/ROM is convenient for analyzing the stability and observing the time response of nonlinear aeroelastic systems, and it is much simpler and more efficient than the full-order CFD simulation.

### C. Adaptation of the POD/ROM

Because the POD/ROM is constructed by small perturbations of the flight parameters (such as the Mach number, Reynolds number, and angle of attack), at a nonlinear steady state solution of the coupled aeroelastic system, it is only accurate when the flight condition is sufficiently close to the nominated steady-state condition. The global POD method [23] and the direct interpolation of the basis vectors [21] were proposed for the adaptation of a POD basis to address parameter variation. However, these approaches have been shown to provide poor results in the transonic regime. Lieu and Farhat [24] proposed a numerical procedure to interpolate the POD bases by means of the subspace-angle interpolation proposed by Golub and Van Loan [25]. Amsallem and Farhat [26] extended the POD basis interpolation method to multivariables with better accuracy based on the matrix approximation algorithm in the tangent space of the Grassmann manifold [27]. Here, we use Amsallem's adaptive POD interpolation method to quickly reconstruct the POD basis under different flow conditions. The following provides a brief introduction to the adaptation algorithm.

Let  $\{S_i\}_{i=0}^{N_R-1}$  denote a set of  $N_\phi$ -dimensional subspaces associated with a set of different operating points of  $\{\lambda_i\}_{i=0}^{N_R-1}$ . These subspaces are represented by their corresponding matrices  $\{\Psi_i \in R^{N_f \times N_\phi}\}_{i=0}^{N_R-1}$ . The new  $N_\phi$ -dimensional subspace  $S_{N_R}$ , associated with a new operating point  $\lambda_{N_R}$ , can be obtained by interpolating the known subspaces  $\{S_i\}_{i=0}^{N_R-1}$  as follows:

$$\begin{aligned} (I - \Psi_{i_0} \Psi_{i_0}^T) \Psi_i (\Psi_{i_0}^T \Psi_i)^{-1} &= U_i \Sigma_i V_i^T \quad (\text{Thin SVD}) \\ \Gamma_i &= U_i \tan^{-1}(\Sigma_i) V_i^T \quad \Gamma_{N_R} = U_{N_R} \Sigma_{N_R} V_{N_R}^T \quad (\text{Thin SVD}) \\ \Psi_{N_R} &= \Psi_{i_0} V_{N_R} \cos(\Sigma_{N_R}) + U_{N_R} \sin(\Sigma_{N_R}) \end{aligned} \quad (15)$$

Once the new POD basis  $\Psi_{N_R}$  is obtained, the new POD/ROM of the aeroelastic system can be updated quickly by Eq. (14). The adaptation procedure specified in the previous algorithm can be described as an interpolation method in the tangent space of a Grassmann manifold, which supports multivariable interpolation, such as the Mach number, angle of attack, dynamic pressure, etc. The details of the interpolation algorithm can be found in [26,27].

### D. ROM Validation

#### 1. Unsteady Responses

The Goland+ wing model is a variant of the heavy Goland wing, which was developed as a transonic-flutter test case by Eastep and Olsen [28]. Based on the original Goland wing, the heavy Goland wing had increased mass to ensure applicability in the transonic regime. The Goland+ wing is modeled with a box structure beam to allow a variety of store attachment options. The wing semispan is 20 ft (6.096 m), the chord is 6 ft (1.8288 m), the thickness-to-chord ratio is 0.04, and the elastic axis is located 2 ft (0.6096 m) from the leading edge. The symmetric airfoil section is constant over the spanwise direction of the wing. Figures 1 and 2 plot the structural model and the aerodynamic surface mesh, respectively. The wing/store system has 200,000 aerodynamic grid points. The infinite plane spline interpolation method is used to deal with the mesh mapping between the flow and structure. The spring-analogy dynamic-mesh algorithm is applied to track the movement of the structure.

One of the key elements of the POD/ROM is the construction of the POD snapshot matrix, which can be calculated from Eq. (13) in the time domain or in the frequency domain. In the time domain, applying the central differential scheme to the snapshot Eq. (5) produces the following form:

$$\frac{w^{n+1} - w^n}{\Delta t} = A \frac{w^{n+1} + w^n}{2} + B y^{n+1/2} \quad (16)$$

This equation can be rearranged as follows:

$$\left(I - \frac{A \Delta t}{2}\right) w^{n+1} = \left(I + \frac{A \Delta t}{2}\right) w^n + B \Delta t y^{n+1/2} \quad (17)$$

For a given input, the time responses or snapshots can be computed from Eq. (17) by the implicit time-marching method. If the order of the structure mode is  $s$ , the number of snapshot vectors is  $m$ ; consequently, the dimension of the snapshot matrix is  $2s \times m$ . Our POD/ROM solver used the Dirac triangle-impulse function for every structural modal displacement and velocity. The solver was successfully used to simulate nonlinear aeroelastic behaviors, such as flutter and limit-cycle oscillation, in cases including the NLR 7301 airfoil model, the AGARD 44.6 wing, and the Goland+ wing [12,16,17].

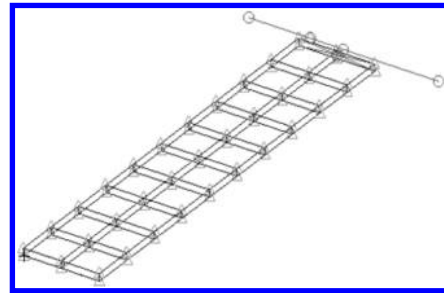


Fig. 1 The structural model of the Goland+ wing.

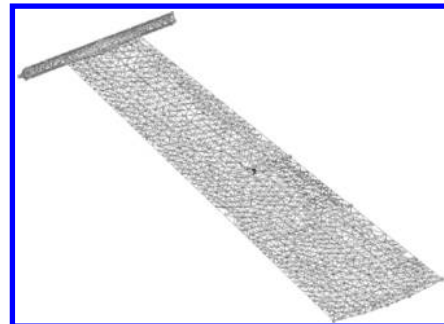


Fig. 2 The aerodynamic surface mesh.

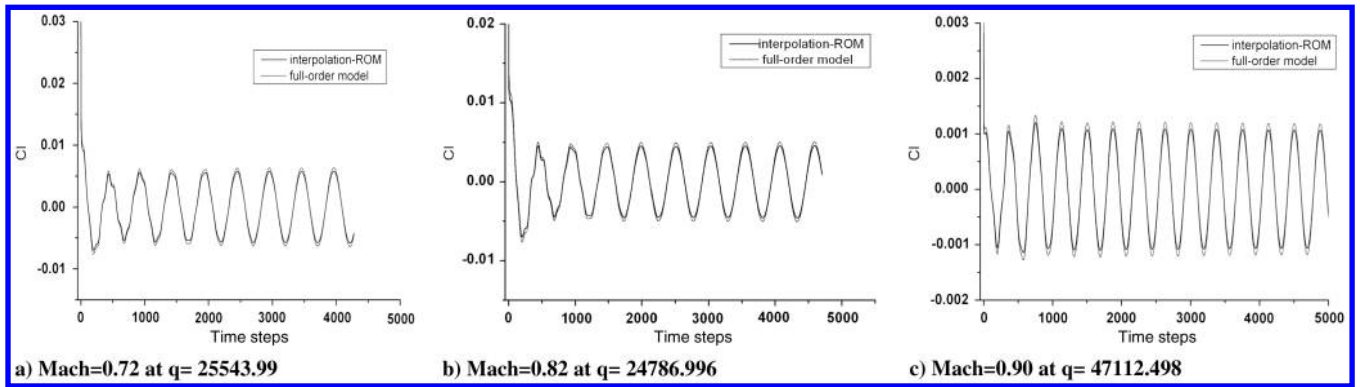


Fig. 3 The aerodynamic responses of the adaptive POD/ROM and the full-order model.

To construct the adaptive POD/ROM, the traditional POD/ROMs for the Goland+ wing should be preconstructed at several selected Mach numbers, such as 0.94, 0.89, 0.86, 0.78, and 0.66. For each chosen Mach number, the state-space snapshot Eq. (17) was first used to compute the snapshots with a time step of  $dt = 5 \times 10^{-5}$  s. The first 300 time-response samples for each model were chosen to construct the snapshot matrix. Second, three different-order POD/ROMs, including 300-order, 80-order, and 60-order ROMs, were constructed. Third, to select an appropriate ROM, the aeroelastic time responses of the Goland+ wing were calculated by the three POD/ROMs and the full-order linearized model with a time step of  $dt = 0.001$  s. An initial vertical velocity of 0.01 was given to the second structural mode. The comparison results showed that the 300-order and 80-order ROMs were sufficient to capture the dominant aeroelastic behavior, whereas the 60-order ROM exhibited obvious differences. Consequently, the lower 80-order POD/ROM was finally chosen for all the Mach numbers. The CFD/CSD-coupled solver took approximately 6 h to compute the structural responses, whereas the POD/ROM only required approximately 2 min on an i7-CPU PC. Even when the cost of building the POD/ROM is considered, the computational efficiency is increased by nearly an order of magnitude.

The preconstructed and verified POD/ROMs were used to update the POD/ROMs under new flow conditions by the interpolation algorithm described in Eq. (15). The unsteady lift coefficient responses of the aeroelastic system at Mach numbers 0.90, 0.82, and 0.72 were calculated to validate the accuracy and efficiency of the adaptive POD/ROM model. Figure 3 shows the simulation results predicted by the adaptive ROM and the full-order model at different Mach numbers and dynamic pressures. The comparisons in Fig. 3 indicate that the adaptive algorithm and the updated ROMs have good efficiency and accuracy for predicting the unsteady aerodynamic responses of the Goland+ wing.

## 2. Flutter-Boundary Prediction

The flutter boundary predicted by the adaptive-interpolation POD/ROM was compared with those presented by Snyder et al. [29] and Parker et al. [30]. From Fig. 4, it can be observed that the flutter boundary predicted by the adaptive POD/ROM agrees well with the full-order model, especially at Mach numbers below 0.91. The comparisons of the time responses of the first structural mode predicted by the adaptive-interpolation ROM with those predicted by the full-order model are illustrated in Figs. 5 and 6, in which the dynamic pressures are 46,112 and 48,112, respectively, below and above the flutter point at Mach 0.9. The stable and unstable time responses of the first mode predicted by the two models agree well. This result indicates that the interpolation of the POD/ROM can also capture the aeroelastic behaviors under new flow conditions with good accuracy.

It takes nearly 1 h for the reconstruction of the new POD/ROM under new flow conditions, whereas only several minutes are required for the interpolation of the POD basis. Considering the high computational efficiency of the updated ROM, although there are

some obvious differences after Mach 0.91, it still provides a good initial value for the accurate prediction by the CFD/CSD-coupled simulation. In addition, more preconstructed ROMs can be added to the database to improve the performance of the adaptive POD/ROM.

The two aforementioned cases indicate that the adaptive POD/ROM can represent the dominant dynamics of the aeroelastic behavior over a broad flight envelope. The POD/ROM provides a potential tool for nearly real-time aeroelastic simulation. In the next section, we develop an LPV aeroservoelastic model based on the adaptive POD/ROM.

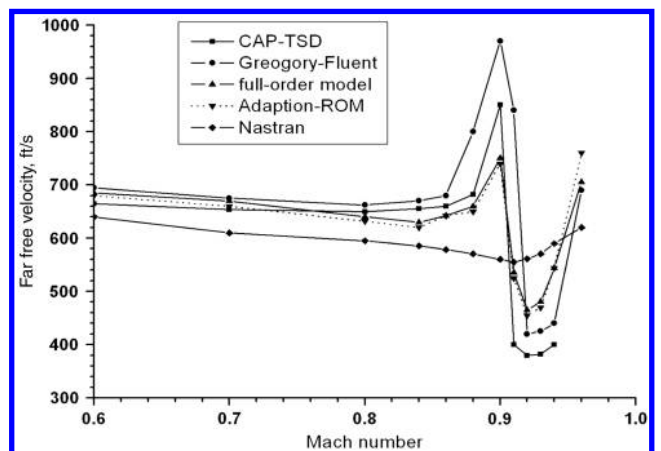


Fig. 4 Comparison of the flutter boundary predicted by different models.

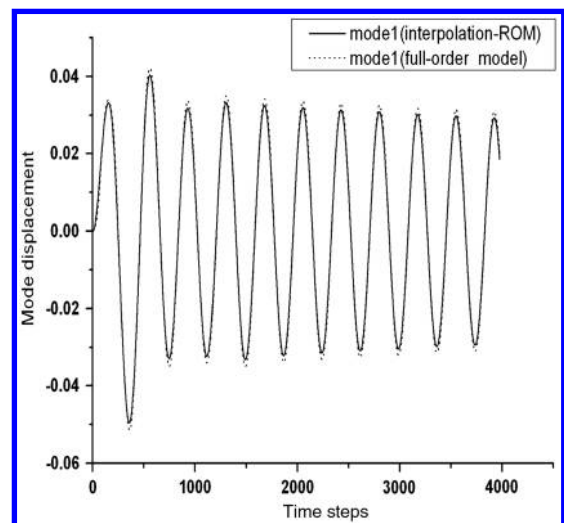


Fig. 5 The stable response at Mach 0.9,  $q = 46112$ .

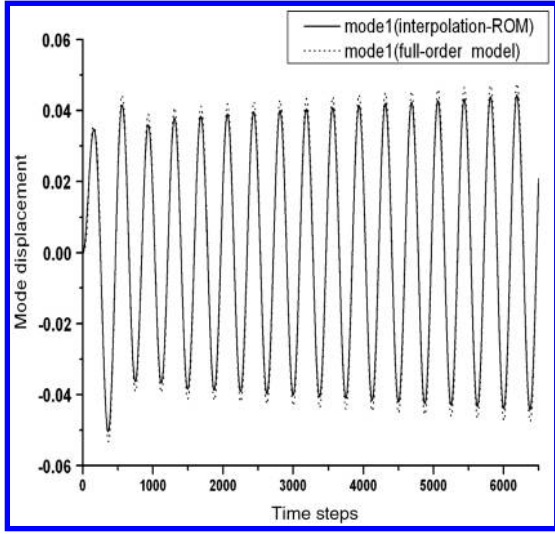


Fig. 6 The unstable response at Mach 0.9,  $q = 48112$ .

### III. LPV Controller Design

#### A. LPV Aeroservoelastic Model for the Goland+ Wing

As a demonstration, one flap-control surface is used to stabilize the dynamic instability of the Goland+ wing aeroelastic model plotted in Fig. 2. The following LPV aeroservoelastic model based on the adaptive POD/ROM is obtained by adding the unsteady aerodynamic perturbation of the flap-control surface into Eq. (14):

$$\begin{aligned} \begin{bmatrix} \dot{w}_r \\ \dot{v} \\ \dot{u} \end{bmatrix} &= \begin{bmatrix} -\Psi_r^T A_0^{-1} H \Psi_r & -\Psi_r^T A_0^{-1} (E + C) & -\Psi_r^T A_0^{-1} G \\ \frac{1}{2} \rho_\infty V_\infty^2 \bar{M}^{-1} P_w \Psi_r & -\bar{M}^{-1} \bar{C} & -\bar{M}^{-1} \bar{K}_S \\ 0 & I & 0 \end{bmatrix} \begin{bmatrix} w_r \\ v \\ u \end{bmatrix} \\ &+ q_\infty \begin{bmatrix} P_{w\beta} \\ P_{f\beta} \\ 0 \end{bmatrix} \beta \end{aligned} \quad (18)$$

where  $\beta$  is the deflection of the flap,  $P_{w\beta}$  is the perturbation matrix of the unit deflection of the flap to the flowfield variables, and  $P_{f\beta}$  is the perturbation matrix of the unit deflection of the flap to the general aerodynamic force. These control matrices can also be precomputed by the unsteady CFD solver to build the POD basis at the given Mach numbers. The control matrices are also dependent on the flight conditions, but their new values at the changed flow parameters can be calculated very quickly by the simple Lagrange interpolation algorithm. The POD basis  $\Psi_r$  is dependent on the Mach number, which can also be updated quickly by the interpolation algorithm described in Sec. II.C. Before constructing the LPV aeroservoelastic model, the POD basis database was previously computed at the selected Mach numbers (i.e., 0.94, 0.89, 0.86, 0.78, and 0.66). Therefore, the LPV aeroservoelastic model can be updated very quickly based on the adaptive POD/ROM method. Finally, the state-space equation of the aeroservoelastic model can be written as follows:

$$\begin{cases} \dot{x} = A(q_\infty, M_\infty)x + B(q_\infty, M_\infty)\beta \\ y = Cx \end{cases} \quad (19)$$

When  $B = 0$ , the LPV aeroelastic equation is obtained. This equation can be used to predict the system response to parameter variation (such as the Mach number or altitude in the flight envelope) in near-real time. For the active control of the aeroelastic system in Eq. (19), the input is the deflection of the control surface  $\beta$ , and the

corresponding output is the structural response, i.e., the modal displacement and the modal velocity. The active control/stability augmentation problem is the design of the control law  $\beta = -K(x)$ , which stabilizes the unstable structural response or enlarges the flight envelope.

#### B. LPV Gain-Scheduled Control-Law Design

The LPV theory offers several advantages over classical gain-scheduled control, in that the resulting LPV controllers are automatically gain scheduled, and no ad hoc methods of gain scheduling are needed. The details of the LPV control theory can be found in the control-theory references; consequently, only a brief description is introduced here. The standard LQR control problem can be represented as the LTI state system described by

$$\dot{x} = Ax + Bu + w \quad z = \begin{bmatrix} Q^{1/2} & 0 \\ 0 & R^{1/2} \end{bmatrix} \begin{bmatrix} x \\ u \end{bmatrix} \quad (20)$$

where  $Q$  and  $R$  are the weightings of the state variables and the input variables, respectively. Equation (20) can be represented in the form of a generalized control problem:

$$\begin{bmatrix} \dot{x} \\ z \\ y \end{bmatrix} = \begin{bmatrix} A & B_1 & B \\ C_1 & D_1 & E_1 \\ C & F_1 & 0 \end{bmatrix} \begin{bmatrix} x \\ w \\ u \end{bmatrix} \quad (21)$$

with  $B_1 = I$ ,  $C_1 = [Q^{1/2} \ 0]^T$ ,  $D_1 = [0 \ 0]^T$ ,  $E_1 = [0 \ R^{1/2}]^T$ ,  $F_1 = 0$ .

For a parameter vector  $p$ , the closed-loop linear parameter-varying state-space form of the generalized control problem of Eq. (21) under the state feedback  $C = I$  with feedback gain  $K(\theta)$  is

$$G(\theta) := \begin{bmatrix} A'(\theta) & B'(\theta) \\ C'(\theta) & D'(\theta) \end{bmatrix} := \begin{bmatrix} A(\theta) + A(\theta)K(\theta) & B_1(\theta) \\ C_1(\theta) + E_1(\theta)K(\theta) & D_1(\theta) \end{bmatrix} \quad (22)$$

With the parameter-dependent Lyapunov variable  $\chi(\theta)$  and the auxiliary parameter  $\lambda(\theta)$ , the  $H_2$  norm of the closed-loop system is  $\|G(\theta)\|_2^2 < \nu$  if the analysis linear matrix inequalities (LMIs) (23) are feasible [31].

$$\begin{cases} \begin{bmatrix} \dot{\chi}(\theta) + A'^T(\theta) + \chi(\theta)A'^T(\theta) & \chi(\theta)B'(\theta)\chi(\theta) \\ B'^T(\theta)\chi(\theta) & -I \end{bmatrix} < 0 \\ \begin{bmatrix} \chi(\theta) & C'^T(\theta) \\ C'(\theta) & \lambda(\theta) \end{bmatrix} > 0, \quad \text{Tr}(\lambda(\theta)) < \nu, \quad D' = 0 \end{cases} \quad (23)$$

For the state-feedback case, a transformed Lyapunov variable  $Y$  and controller variable  $M$  are introduced. When the congruence transformation proposed by Scherer [32] is applied to Eq. (24), the following synthesis LMIs are obtained:

$$\begin{cases} \begin{bmatrix} -\dot{Y}(\theta) + \tilde{A}(\theta) + \tilde{A}(\theta)^T & \tilde{B}(\theta) \\ \tilde{B}(\theta)^T & -I \end{bmatrix} < 0 \\ \begin{bmatrix} Y(\theta) & \tilde{C}^T(\theta)^T \\ \tilde{C}(\theta) & Z(\theta) \end{bmatrix} > 0, \quad \text{Tr}(Z(\theta)) < \nu, \quad \tilde{D} = 0 \end{cases} \quad (24)$$

where the new variables are

$$\begin{bmatrix} \tilde{A}(\theta) & \tilde{B}(\theta) \\ \tilde{C}(\theta) & \tilde{D}(\theta) \end{bmatrix} := \begin{bmatrix} A(\theta)Y(\theta) + B(\theta)M(\theta) & B_1(\theta) \\ C_1(\theta)Y(\theta) + E_1(\theta)M(\theta) & D_1(\theta) \end{bmatrix} \quad (25)$$

Now, the synthesis LMIs are affine in the variables  $Y(\theta)$  and  $M(\theta)$ . The Lyapunov matrix and the gain of the controller can be calculated as follows:

$$\chi(\theta) = Y^{-1}(\theta), \quad K(\theta) = M(\theta)Y^{-1}(\theta) \quad (26)$$

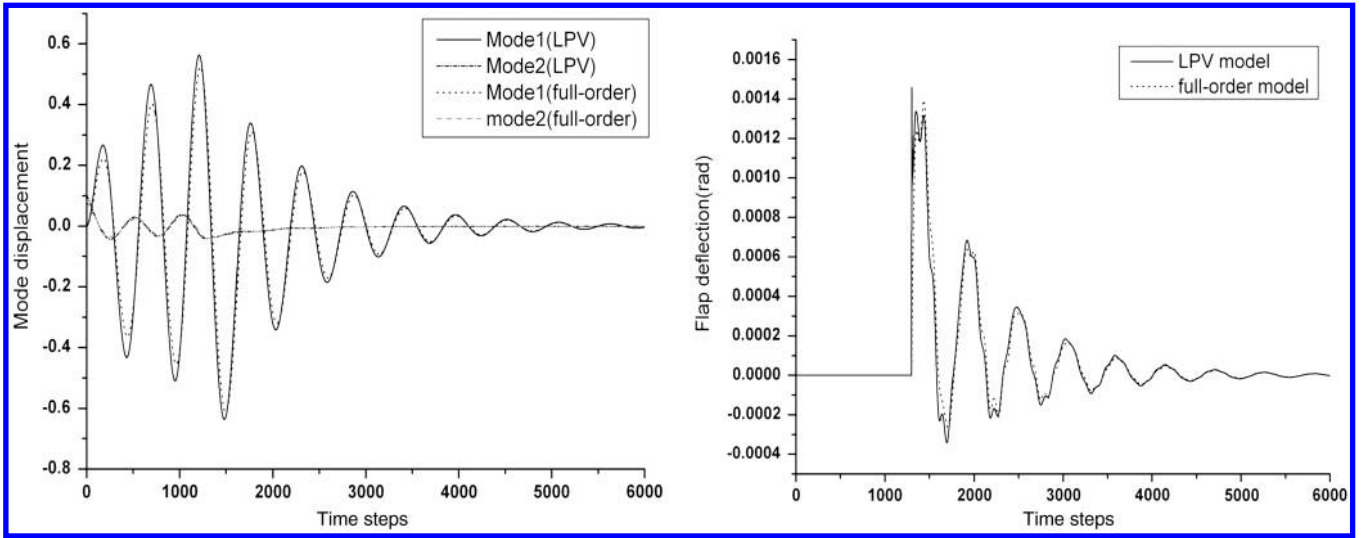


Fig. 7 Comparison of the controlled aeroelastic response at Mach 0.72,  $q = 31041.56$ .

### IV. Simulation and Results

#### A. Controlled Response of Different Parameters

The time response of the Golland+ wing at Mach 0.72 and a dynamic pressure of 31041.56 are illustrated in Fig. 7. The dynamic

pressure is above the flutter point; thus, the system becomes divergent very quickly without control. The system stabilizes quickly after the controller is started at the 1300th time step of the simulation. The deflection of the control flap is also smooth, which is good for the

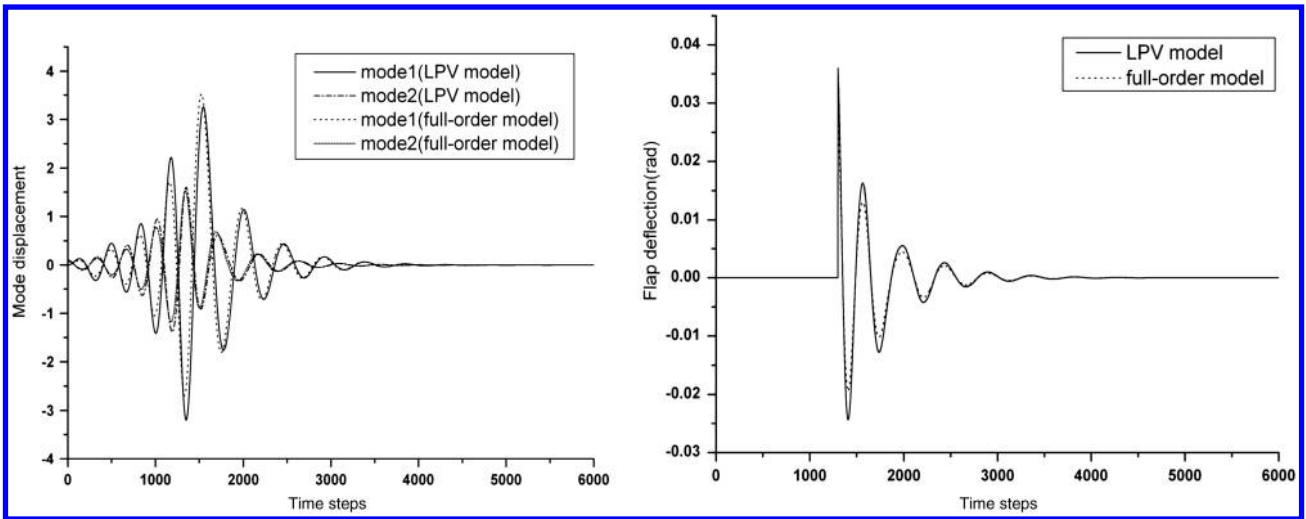


Fig. 8 Comparison of the controlled aeroelastic response at Mach 0.92,  $q = 20458.12$ .

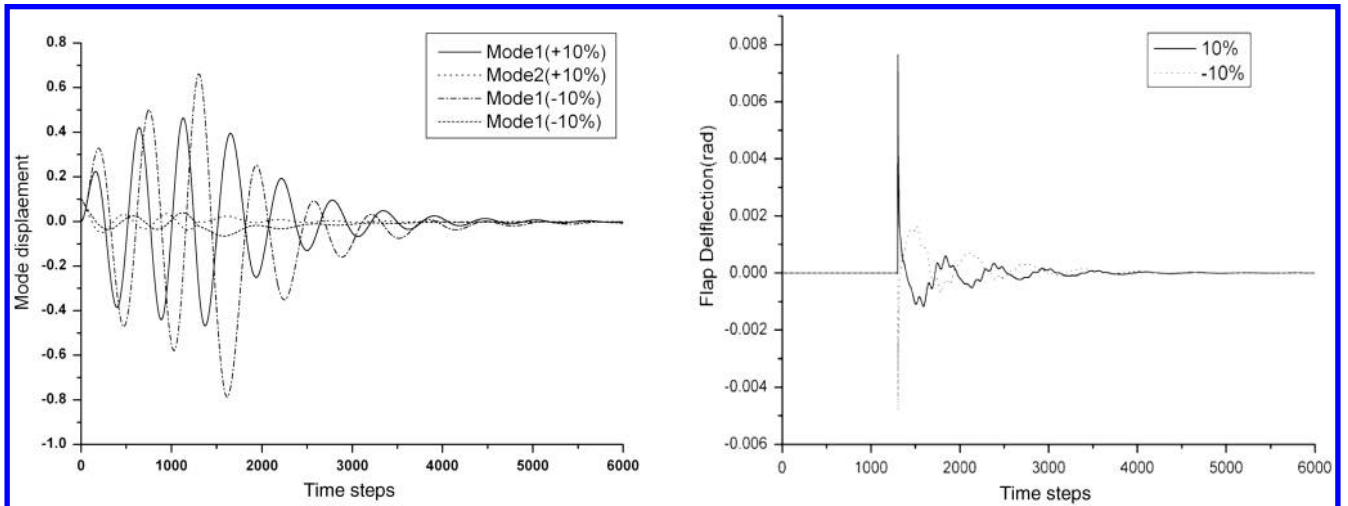


Fig. 9 Aeroelastic response at Mach 0.72,  $q = 31041.56$ .

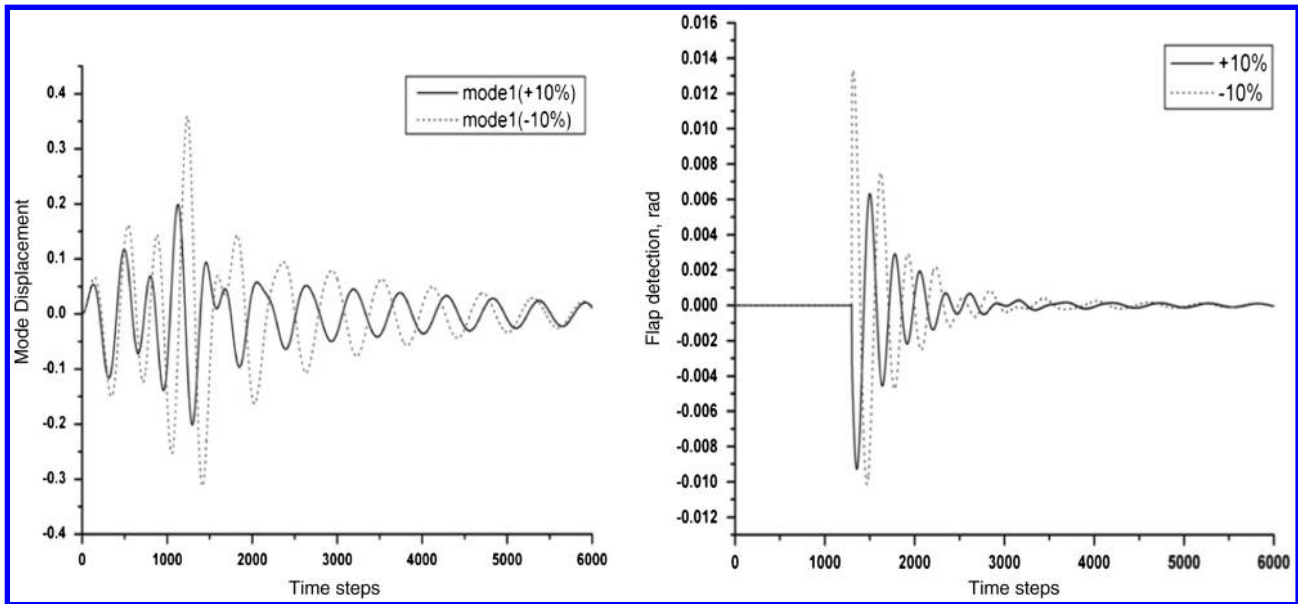


Fig. 10 Aeroelastic response at Mach 0.92,  $q = 8654$ .

practical physical realization. Figure 8 illustrates the aeroelastic response with the LPV controller at Mach 0.92 and a dynamic pressure of 20485.12, which is also above the flutter point. The divergent Goland+ wing can also be well suppressed after starting the active controller at the 1300th time step.

Figures 7 and 8 also show that the aeroelastic time responses predicted by the LPV model agree well with the full-order model, which demonstrates the capacity and efficiency of the LPV model. The most important advantage is that the control gain is autoscheduled without an explicit assignment. As a benefit of the LPV model, the near-real-time aeroservoelastic simulation of flexible aircraft based on high-fidelity CFD tools becomes possible.

### B. Robust Simulation

The robustness of a controller is important because it is impossible to build an absolutely accurate plant model, and model errors always exist. Robustness is also important because the properties of the structure may change during flight, such as the separation of the wing-tip store. Consequently, an analysis of the robustness of the active controller is required. By allowing the structural stiffness to change by  $\pm 10\%$ , Figs. 9 and 10 show the aeroelastic responses with the LPV controller from the 1300th time step at Mach 0.72 and 0.92, respectively. The simulation results indicate that the designed LPV controller can still successfully suppress the unstable system with good performance.

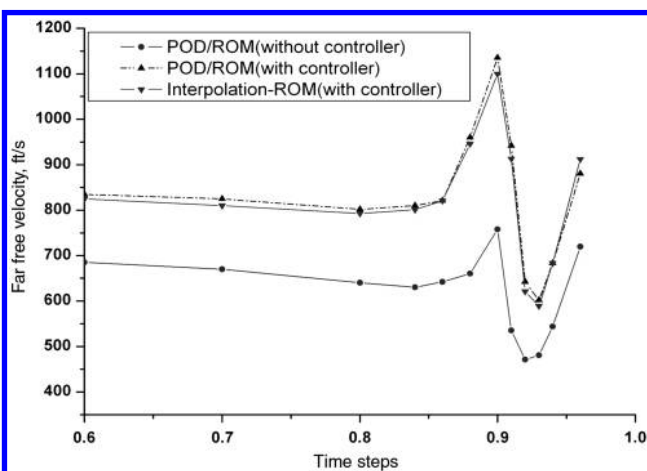


Fig. 11 Controlled and uncontrolled flutter boundary.

### C. Comparison of the Predicted Flutter Boundary

The other performance criterion for controller evaluation is the improvement of the flutter boundary. The flutter boundaries with and without the LPV controller are compared in Fig. 11, which shows that an enhancement of approximately 20–30% was obtained for the active LPV controller. The controlled flutter boundary predicted by the interpolation adaptive ROM is very close to that of the POD/ROM, especially at the previously selected operation points at which the POD basis was preconstructed. This result implies that the LPV model is suitable for designing the active control law because of its good representation of the dynamic behaviors of the Goland+ wing over a wide range of the flight regime.

## V. Conclusions

A new general linear parameter-varying aeroservoelastic model based on the adaptive proper orthogonal decomposition reduced-order model was investigated. The linear parameter-varying model enabled the use of linear parameter-varying control theory to design a robust and implicit gain-scheduled flutter controller. The method proposed a general framework for the physics-based high-fidelity numerical simulation method to be applied to the design of active flutter-suppression control laws. The linear parameter-varying model was also able to deal with the time-varying flow parameters in the flight envelope with nonlinear aerodynamic effects in the transonic regime. The proposed method is a promising method and an attractive tool for integrated flight simulation, which combines rigid flight dynamics with the aeroelastic dynamics of a flexible aircraft based on high-fidelity computational fluid dynamics tools.

### Acknowledgments

This work was partially supported by the National Natural Science Foundation of China (10902082, 91016008), the New Faculty Research Foundation of Xi'an Jiaotong University, and the Fundamental Research Funds for the Central Universities (xjj20100126). The first author would like to thank Thomas Strganac and Qin Z. M. for their helpful comments on the manuscript.

### References

- [1] Mukhopadhyay, V., "Historical Perspective on Analysis and Control of Aeroelastic Responses," *Journal of Guidance, Control, and Dynamics*, Vol. 26, No. 5, 2003, pp. 673–684. doi:10.2514/2.5108
- [2] Platanitis, G., and Strganac, T. W., "Control of a Nonlinear Wing Section Using Leading- and Trailing-Edge Surfaces," *Journal of*

- Guidance, Control, and Dynamics*, Vol. 27, No. 1, 2004, pp. 52–58. doi:10.2514/1.9284
- [3] Prime, Z. D., Cazzolato, B. S., Doolan, C. J., and Strganac, T., “Linear-Parameter-Varying Control of an Improved Three-Degree-of-Freedom Aeroelastic Model,” *Journal of Guidance, Control, and Dynamics*, Vol. 33, No. 2, 2010, pp. 615–618. doi:10.2514/1.45657
- [4] ZONA Technology, Inc., “ZAERO User’s Manual,” Ver. 7.3, Scottsdale, AZ, Oct. 2005.
- [5] Baldwin, D., Chen, P., Panza, J., and Adams, J., “Unified Rational Function Approximation Formulation for Aeroelastic and Flight Dynamics Analyses,” 47th AIAA/ASME/ASCE/AHS/ASC Structures, Structural Dynamics, and Materials Conference, Newport, RI, AIAA Paper 2006-2025, May 2006.
- [6] Lucia, D. J., Beran, P. S., and Silva, W. A., “Reduced-Order Modeling: New Approaches for Computational Physics,” *Progress in Aerospace Sciences*, Vol. 40, No. 1, 2004, pp. 51–117. doi:10.1016/j.paerosci.2003.12.001
- [7] Silva, W. A., and Bartels, R. E., “Development of Reduced-Order Models for Aeroelastic Analysis and Flutter Prediction Using the CFL3Dv6.0 Code,” *Journal of Fluids and Structures*, Vol. 19, No. 6, 2004, pp. 729–745. doi:10.1016/j.jfluidstructs.2004.03.004
- [8] Cowan, T. J., Arena, A. S., and Gupta, K. K., “Accelerating Computational Fluid Dynamics Based Aeroelastic Predictions Using System Identification,” *Journal of Aircraft*, Vol. 38, No. 1, 2001, pp. 81–87. doi:10.2514/2.2737
- [9] Thomas, J. P., Dowell, E. H., and Hall, K. C., “Three-Dimensional Transonic Aeroelasticity Using Proper Orthogonal Decomposition-Based Reduced-Order Models,” *Journal of Aircraft*, Vol. 40, No. 3, 2003, pp. 544–551. doi:10.2514/2.3128
- [10] Thomas, J. P., Dowell, E. H., and Hall, K. C., “Modeling Viscous Transonic Limit-Cycle Oscillation Behavior Using a Harmonic Balance Approach,” *Journal of Aircraft*, Vol. 41, No. 6, 2004, pp. 1266–1274. doi:10.2514/1.9839
- [11] Woodgate, M. A., Badcock, K. J., “Fast Prediction of Transonic Aeroelastic Stability and Limit Cycles,” *AIAA Journal*, Vol. 45, No. 6, 2007, pp. 1370–1381. doi:10.2514/1.25604
- [12] Chen, G., Li, Y. M., and Yan, G. R., “A Nonlinear POD Reduced Order Model for Limit Cycle Oscillation Prediction,” *Science in China. Series G: Physics, Mechanics and Astronomy*, Vol. 53, No. 7, 2010, pp. 1325–1332. doi:10.1007/s11433-010-4013-2
- [13] Marzocca, P., Silva, W. A., and Libreseu, L., “Nonlinear Open/Closed-Loop Aeroelasticity for Airfoils via Volterra Series Approach,” *AIAA Journal*, Vol. 42, No. 4, 2004, pp. 673–686. doi:10.2514/1.9552
- [14] Allen, C., Fenwick, C., Taylor, N., and Djayapertapa, L., “Investigation of Flutter Suppression by Active Control,” 21st AIAA Applied Aerodynamics Conference, Orlando, FL, AIAA Paper 2003-3510, June 2003.
- [15] Zhang, Z. J., Min, X., and Chen, S. L., “Active Flutter Control of Transonic Flapped Wing Based on CFD/CSD Coupling,” *Proceedings of the 7th International Conference on System Simulation and Scientific Computing*, IEEE Publ., Piscataway, NJ, Oct. 2008, pp. 430–435.
- [16] Gang, C., Yuemin, L., and Guirong, Y., “Active Control Stability/Augmentation System Design Based on Reduced Order Model,” *Chinese Journal of Aeronautics*, Vol. 23, No. 6, 2010, pp. 637–644. doi:10.1016/S1000-9361(09)60265-X
- [17] Chen, G., Li, Y. M., Yan, G. R., and Xu, M., “Design of Active Control Law for Aeroelastic Systems via Reduced Order Models,” *Acta Aeronautica et Astronautica Sinica*, Vol. 31, No. 1, 2010, pp. 12–18 (in Chinese).
- [18] Packard, A., and Kantner, M., “Gain Scheduling the LPV Way,” *Proceedings of the 35th IEEE Control Decision Conference*, IEEE Publ., Piscataway, NJ, 1996, pp. 3938–3941.
- [19] Barker, J. M., Balas, G. J., and Blue, P. A., “Gain-Scheduled Linear Fractional Control for Active Flutter Suppression,” *Journal of Guidance, Control, and Dynamics*, Vol. 22, No. 4, 1999, pp. 507–512. doi:10.2514/2.4418
- [20] Lieu, T., Farhat, C., and Lesoinne, M., “POD-Based Aeroelastic Analysis of a Complete F-16 Configuration: ROM Adaptation and Demonstration,” 46th AIAA/ASME/ASCE/AHS/ASC Structures, Structural Dynamics and Materials Conference, Austin, TX, AIAA Paper 2005-2295, April 2005.
- [21] Farhat, C., Geuzaine, P. and Brown, G., “Application of a Three-Field Nonlinear Fluid-Structure Formulation to the Prediction of the Aeroelastic Parameters of an F-16 Fighter,” *Computers and Fluids*, Vol. 32, No. 1, 2003, pp. 3–29. doi:10.1016/S0045-7930(01)00104-9
- [22] Holmes, P., Lumley, J. L., and Berkooz, G., *Turbulence, Coherent Structures, Dynamical Systems and Symmetry*, Cambridge Univ. Press, Cambridge, England, U.K., 1996, pp. 93–96.
- [23] Schmidt, R., and Glauser, M., “Improvements in Low Dimensional Tools for Flow-Structure Interaction Problems: Using Global POD,” 42nd AIAA Aerospace Sciences Meeting and Exhibit, Reno, NV, AIAA Paper 2004-0889, Jan. 2004.
- [24] Lieu, T., and Farhat, C., “Adaptation of Aeroelastic Reduced-Order Models and Application to an F-16 Configuration,” *AIAA Journal*, Vol. 45, No. 6, 2007, pp. 1244–1257. doi:10.2514/1.24512
- [25] Golub, G. H., and Van Loan, C. F., *Matrix Computations*, 2nd ed., John Hopkins Univ. Press, Baltimore, MD, 1989.
- [26] Amsallem, D., and Farhat, C., “Interpolation Method for Adapting Reduced-Order Models and Application to Aeroelasticity,” *AIAA Journal*, Vol. 46, No. 7, 2008, pp. 1803–1813. doi:10.2514/1.35374
- [27] Edelman, A., Arias, T. A., and Smith, S. T., “The Geometry of Algorithms with Orthogonality Constraints,” *SIAM Journal on Matrix Analysis and Applications*, Vol. 20, No. 2, 1998, pp. 303–353. doi:10.1137/S0895479895290954
- [28] Eastep, F. E., and Olsen, J. J., “Transonic Flutter Analysis of a Rectangular Wing with Conventional Airfoil Sections,” *AIAA Journal*, Vol. 18, No. 10, 1980, pp. 1159–1164. doi:10.2514/3.50866
- [29] Snyder, R. D., Scott, J. N., Khot, N. S., Beran, P., and Zwebner, J., “Predictions of Store-Induced Limit-Cycle Oscillations Using Euler and Navier–Stokes Fluid Dynamics,” 44th AIAA/ASME/ASCE/AHS/ASC Structures, Structural Dynamics, and Materials Conference, Norfolk, VA, AIAA Paper 2003-1727, April 2003.
- [30] Parker, G. H., Maple, R. C., and Beran, P. S., “Analysis of Store Effects on Limit-Cycle Oscillation,” 47th AIAA/ASME/ASCE/AHS/ASC Structures, Structural Dynamics, and Materials Conference, Newport, RI, AIAA Paper 2006-1846, May 2006.
- [31] Xie, W., “H2 Gain Scheduled State Feedback for LPV System with New LMI Formulation,” *Control Theory and Applications*, Vol. 152, No. 6, 2005, pp. 693–697. doi:10.1049/ip-cta:20050052
- [32] Scherer, C. W., “Robust Mixed Control and Linear Parameter-Varying Control with Full Block Scalings,” *Advances in Linear Matrix Inequality Methods in Control*, Society for Industrial and Applied Mathematics, Philadelphia, 2000, Chap. 10, pp. 87–208.